Environmental Science & Technology

Article

Cite This: Environ. Sci. Technol. 2019, 53, 8017−8026

pubs.acs.org/est

Atmospheric Concentrations and Wet/Dry Loadings of Mercury at the Remote Experimental Lakes Area, Northwestern Ontario, Canada

Vincent L. St. Louis,*[,†] Jennifer A. Graydon,[†] Igor Lehnherr,[‡] Helen M. Amos,[§] Elsie M. Sunderland,[§,∥] Kyra A. St. Pierre,[†] Craig A. Emmerton,[†] Ken Sandilands,[⊥] Michael Tate,[#] Alexandra Steffen,[▽] and Elyn R. Humphreys[○]

[†]Department of Biological Sciences, University of Alberta, Edmonton, Alberta T6G 2E9, Canada

[‡]Department of Geography, University of Toronto-Mississauga, 3359 Mississauga Road, Mississauga, Ontario L5L 1C6, Canada

[§]Harvard T.H. Chan School of Public Health, Department of Environmental Health, Boston, Massachusetts 02215, United States

[∥]Harvard John A. Paulson School of Engineering and Applied Sciences, Cambridge, Massachusetts 02138, United States

[⊥]International Institute of Sustainable Development − Experimental Lakes Area (IISD-ELA), 111 Lombard Avenue, Suite 325, Winnipeg, Manitoba R3B 0T4, Canada

[#]University of Wisconsin, Aquatic Science Center, 1975 Willow Drive, Madison, Wisconsin 53706, United States

[▽]Environment and Climate Change Canada, Science and Technology Branch, Air Quality Research, 4905 Dufferin Street, Toronto, Ontario M3H 5T4, Canada

[○]Department of Geography and Environmental Studies, Carleton University, Ottawa, Ontario K1S 5B6, Canada

Supporting Information

ABSTRACT: Mercury (Hg) is a global pollutant released from both natural and human sources. Here we compare long-term records of wet deposition loadings of total Hg (THg) in the open to dry deposition loadings of THg in throughfall and litterfall under four boreal mixedwood canopy types at the remote Experimental Lakes Area (ELA) in Northwestern Ontario, Canada. We also present long-term records of atmospheric concentrations of gaseous elemental (GEM), gaseous oxidized (GOM), and particle bound (PBM) Hg measured at the ELA. We show that dry THg loadings in throughfall and litterfall are 2.7 to 6.1 times greater than wet THg loadings in the open. GEM concentrations showed distinct monthly and daily patterns, correlating positively in spring and summer with rates of gross ecosystem productivity and respiration. GOM and PBM concentrations were less variable throughout the year but were highest in the winter, when concentrations of anthropogenically sourced particles and gases were also high. Forest fires, Arctic air masses, and road salt also impacted GEM, GOM, and PBM concentrations at the ELA. A nested GEOS-Chem simulation for the ELA region produced a dry/wet deposition ratio of >5, suggesting that the importance of dry deposition in forested regions can be reasonably modeled by existing schemes for trace gases.

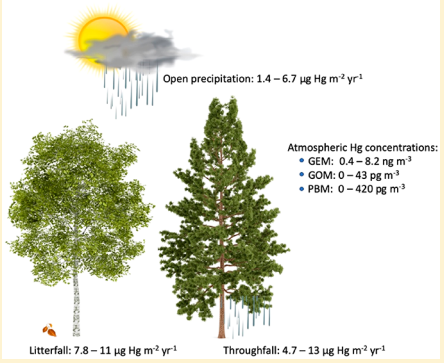

INTRODUCTION

Methylmercury (MeHg) is a global dietary health concern for humans due to the enhanced anthropogenic release of Hg.[1] This has triggered the ratification of the Minamata Convention on Mercury, a global treaty on Hg release to protect human health and the environment.[2] The Convention draws attention to the fact that Hg has had broad uses in everyday products and is released to the atmosphere, soil, and water from a variety of sources. Controlling the anthropogenic releases of Hg has been a key factor in shaping the obligations under the Convention because several studies have shown a positive relationship between Hg loadings to freshwaters and the amount of MeHg subsequently produced in lakes and biomagnified through aquatic foodwebs (e.g., refs 3−5).

Wet deposition monitoring networks have been established in numerous countries around the world to quantify Hg loadings from the atmosphere. However, loadings of Hg to watersheds via dry deposition can be many times greater than loadings in precipitation.[6−8] Dry deposition of Hg to watersheds occurs through foliar uptake of gaseous elemental Hg (GEM) as well as scavenging of gaseous oxidized inorganic Hg (GOM) and particle-bound Hg (PBM) onto reactive surfaces such as forest canopies.[9,10] Quantifying excess Hg

Received: March 3, 2019
Revised: June 17, 2019
Accepted: June 18, 2019
Published: June 18, 2019

DOI: 10.1021/acs.est.9b01338
Environ. Sci. Technol. 2019, 53, 8017−8026

loadings under forest/shrub canopies in litterfall and throughfall relative to loadings in nearby open areas in precipitation provides a method for estimating Hg loadings in a forested watershed due to dry deposition.[11−14]

Hg dry deposition rates can also be readily modeled using several approaches. Chemical transport models for Hg such as GEOS-Chem use a "big leaf" resistance-in-series model designed to calculate the loss from the atmosphere using the composite characteristics of terrestrial surfaces.[15] Alternately, an empirically based estimate of dry deposition can be constructed using atmospheric concentrations of GEM, GOM, and PBM measured using, for example, Tekran Hg speciation air monitoring instrumentation, dry deposition velocities (V_d) based on dominant vegetation types in the watershed, and local meteorological conditions.[16]

The exchange of GEM between the atmosphere and vegetation is unique in that it can be bidirectional depending on atmospheric concentrations. In general, there is thought to be a net stomatal uptake of GEM during periods of gross ecosystem productivity (GEP).[7,9] The atmospheric exchange of GOM and PBM with vegetation tends to be a one-way flux downward, unless there is photoreduction of GOM following deposition on foliar surfaces.[17] Similar to well-studied chemical species like nitric acid, V_d values for GEM range between 0.1 and 0.4 cm s^{-1} over vegetated surfaces like forests and wetlands but are much lower over nonvegetated surfaces and soils below canopies.[16] Measurements for GOM deposition are more limited and variable but suggest that because of its reactivity, GOM is readily deposited to most surfaces with V_d values ranging between 0.5 and 6 cm s^{-1}.[16] The deposition of PBM is relatively understudied, with limited data suggesting V_d values in the range of 0.02 to 2 cm s^{-1}.[16] In temperate and northern regions, V_d values also show seasonal variation due to seasonal variations in parameters such as leaf area indexes (LAIs), such that V_d values are often much lower in the winter than in the summer in mixedwood and deciduous forest regions.

During various periods between 2001 and 2013, we quantified wet and dry (net throughfall plus litterfall) loadings of total Hg (THg; all forms of Hg in a sample), as well as atmospheric concentrations of GEM, GOM, and PBM, at the Experimental Lakes Area (ELA) in the remote boreal mixedwood ecoregion of Northwestern Ontario, Canada (Figure S1). In this study, we: (1) extend a previously published record of wet, throughfall, and litterfall loadings of THg at the ELA (ref 14) to now include 2001−2010; (2) discuss 8 years (2005−2013) of atmospheric GEM, GOM, and PBM concentrations data collected at this remote location; (3) use those atmospheric Hg concentrations to model dry THg loadings; and (4) compare measured and modeled estimates of dry THg loadings to determine the best steps forward for effectively and efficiently quantifying Hg wet and dry deposition loadings to watersheds.

METHODS

Field Sites. During our study period, the ELA was operated by the Department of Fisheries and Oceans Canada but is now operated by the International Institute of Sustainable Development (www.iisd.org/ela/). Our research was conducted at two ELA locations (Figure S1). The first location was the ELA meteorological station (Meteorological Service of Canada designation: Rawson Lake Station; Environment and Climate Change Canada (ECCC)) situated ∼0.5 km northwest of the ELA base station on a bedrock knoll ridge with a 1.13 ha oval-shaped forest clearing (49°39.50′ N; 93°43.16′ W; elevation 369 m.a.s.l.). The surrounding boreal mixedwood forest consisted of jack pine (*Pinus banksiana*) and white birch (*Betula papyrifera*) regenerated following an intense 1980 forest fire. The second location was in the Lake 658 watershed (49°43.95′ N; 93°44.2′ W), where the Mercury Experiment to Assess Atmospheric Loadings in Canada and the U.S. (METAALICUS) was conducted.[3] Lake 658 is 8 ha in surface area with a 43 ha catchment. Six ha of the NW catchment were logged in 1978 and supported a deciduous forest of red maple (*Acer rubrum*) and white birch. A 1983 fire burned most of the south side of the watershed and a portion of the north shore. This 21 ha burned area contained a dense canopy of regenerated jack pine. The 14 ha portion of the upland that was not burned or logged was dominated by old growth black spruce (*Picea mariana*) and balsam fir (*Abies balsamea*). A 2 ha wetland connected to the west end of the lake contained a canopy of black spruce, jack pine, and alder (*Alnus* sp.) shrubs.

Collection, Analyses, and Calculation of Open Area Precipitation, Throughfall, and Litterfall Loadings. Details of open area precipitation, throughfall, and litterfall collection and analytical protocols were previously published[6,14] but are also detailed in the Supporting Information (SI). Throughfall and litterfall were collected under old growth, jack pine, deciduous, and wetland forest canopy types.

Atmospheric Concentrations of GEM, GOM, and PBM. Atmospheric concentrations of GEM, GOM and PBM were continuously measured at the ELA meteorological station from May 2005 to April 2013 using Tekran Mercury 2537A, 1130 and 1135 units (Figure S1). The 2537A analytical and pump units were housed inside a temperature-regulated (∼21 °C) building. The 1130 and 1135 speciation units were mounted on a nearby tower centrally located in the station clearing, with the intake 1.5 m above exposed granite bedrock. Details of the Tekran operating parameters and sampling rates are provided in the SI. All data were quality-controlled using the Environment and Climate Change Canada Research Data Management and Quality Control (RDMQ) system.[18]

Modeled Dry Deposition. Empirical estimates of dry THg loadings to ELA watersheds (F; ng m^{-2} s^{-1}) were calculated based on atmospheric concentrations (C) of GEM (ng m^{-3}), GOM (pg m^{-3}), or PBM (pg m^{-3}) measured at the ELA using the Tekran system and modeled deposition velocities (V_d, m s^{-1})

$$F = C \times V_d$$

V_d for GEM was modeled using the approach of Wright and Zhang.[19] V_d values for GOM and PBM were modeled using the approach of Zhang et al.[20,21] Canopy surface characteristics (e.g., LAI, stomatal resistance) and meteorological conditions (e.g., moisture, temperature, solar radiation) drive V_d values in given regions.[16] For our site, all V_d values were calculated using a land cover of 25% conifer and 75% mixedwood forest, as in Zhang et al.,[21] which is generally representative of the region given that forest cover is constantly in flux due to forest fires, succession, and logging (e.g., ref 17). Many of the meteorological parameters used in the model to calculate V_d values were measured and recorded every 5 min within 10 m from the Tekran intake using an array of sensors (temperature (HygroClip-S3), relative humidity (HygroClip-S3-XT), wind speed (Met One 014 3-cup anemometer), barometric pressure (Young 61205 V), precipitation volume and timing (CS700 rain gauge)) and a CR10X datalogger (Campbell Scientific

DOI: 10.1021/acs.est.9b01338
Environ. Sci. Technol. 2019, 53, 8017−8026

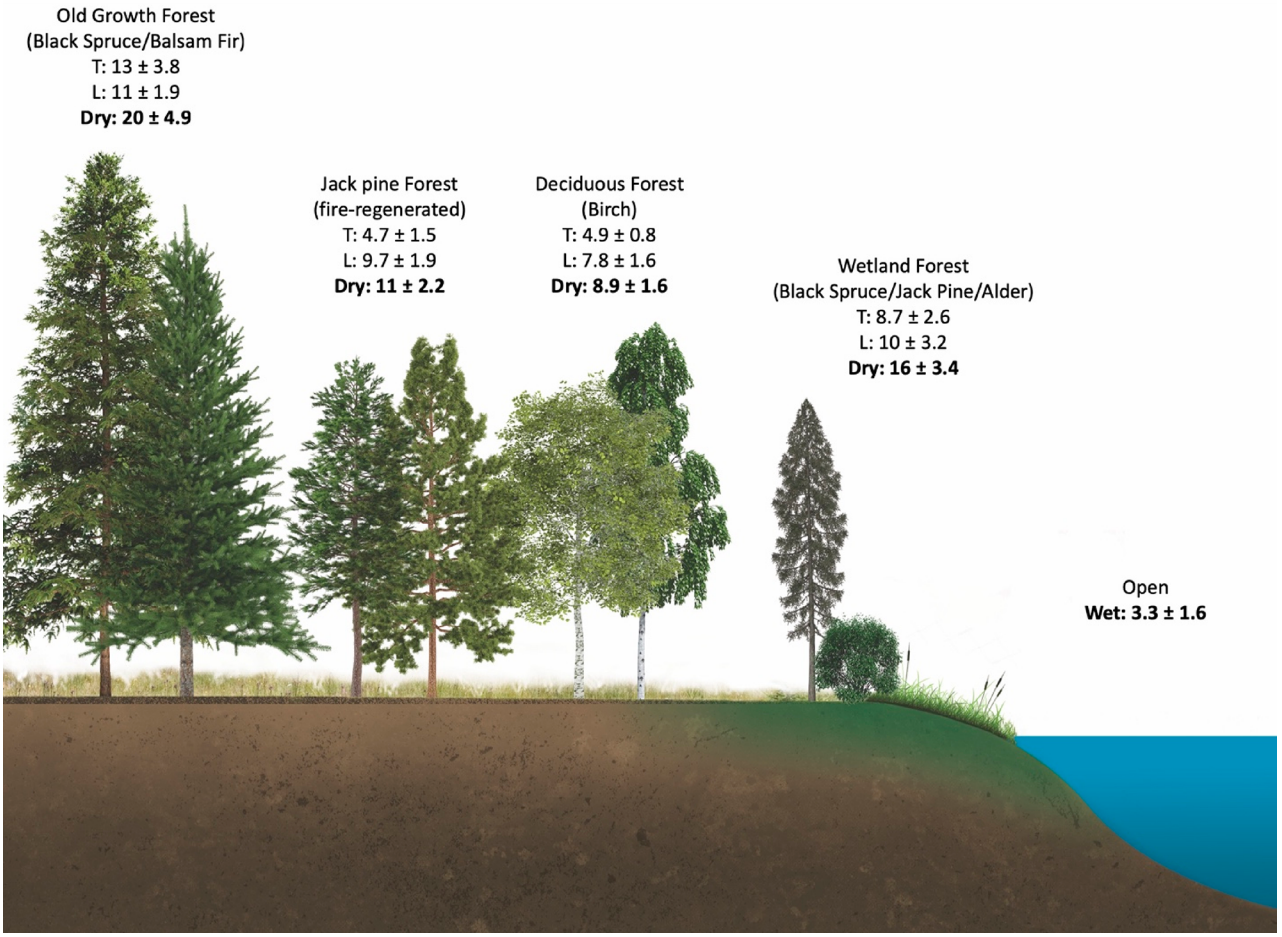

Figure 1. Mean deposition of total Hg (μg m^{-2} yr^{-1}) in the open and under different forest canopies as throughfall (T) and litterfall (L) for the years 2001−2010.

Canada). Snow depth was measured hourly during the winter with a Campbell Scientific SR50-L snow depth sensor. Three hour averages of solar radiation and cloud fraction, which were not measured on-site, were acquired from NASA GEOS-5 assimilated meteorological fields for 2006−2012. Five minute meteorological station data and hourly snow depths were merged with the 3 h GEM, GOM, or PBM data. The 3 h average solar radiation and cloud fraction were interpolated to hourly resolution and also merged with the GEM, GOM, or PBM data.

For comparison, modeled monthly mean dry deposition fluxes of GEM, GOM, and PBM for 2005−2010 were also extracted from archived nested-grid GEOS-Chem simulations.[21] GEOS-Chem is a 3D global chemical transport model with Hg cycling.[22] Zhang et al.[21] simulated Hg deposition over North America using a nested grid with 1/2 × 2/3 degree horizontal resolution. The dry deposition of Hg in GEOS-Chem follows the resistance-in-series scheme from Wesely et al.[15]

RESULTS AND DISCUSSION

Open Area, Throughfall, and Litterfall Loadings of THg. The average annual wet loadings of THg in the open from 2001 to 2010 were 3.3 ± 1.6 μg m^{-2} (Figure 1 and Figure S2). The annual wet loadings of THg at our remote ELA site were 2.6 times lower than those in more populated areas of the nearby Great Lakes region and its subregions (2002−2008 median: 8.6 μg m^{-2}).[23] The wet loadings of THg in the open increased only 0.046 μg m^{-2} yr^{-1} from 2001 to 2010 at the ELA (Figure S3). However, when 2001 loadings were removed from the linear regression analysis (the deployment of precipitation collectors was delayed in our first year of measurements, resulting in annual 2001 loadings being calculated from fewer early season volume-weighted THg concentrations in rain), wet loadings of THg in the open increased 0.352 μg m^{-2} yr^{-1} (Figure S3). This is in contrast with wet loadings of THg in the Great Lakes region and subregions, which did not change between 2002 and 2008.[23] There was no relationship between annual loadings of THg and average annual atmospheric concentrations of GEM (r = 0.009; P = 0.988), GOM (r = −0.103; P = 0.869), and PBM (r = −0.257; P = 0.677) (see below) for years that they were coincidently measured at the ELA (2006−2010) (Pearson product−moment correlation; n = 5).

Throughfall THg loadings were generally 1.4 to 3.8 times higher than THg loadings in the open (Figure 1 and Figure S2). On average, annual throughfall THg loadings were 12.6 ± 3.8, 4.7 ± 1.5, 4.9 ± 0.8, and 8.7 ± 2.6 μg m^{-2} under the old growth, jack pine, deciduous, and wetland forest canopies, respectively (Figure 1 and Figure S2). Litterfall represented another large annual input of THg to catchments, but unlike throughfall loadings, litterfall loadings were relatively similar under old growth (10.8 ± 1.9 μg m^{-2}), jack pine (9.7 ± 1.9 μg m^{-2}), deciduous (7.8 ± 1.6 μg m^{-2}), and wetland (10.3 ± 3.2

DOI: 10.1021/acs.est.9b01338
Environ. Sci. Technol. 2019, 53, 8017−8026

μg m^{-2}) forest canopies (Figure 1 and Figure S2). Although throughfall and litterfall collectors were deployed under similar forest canopy types throughout the study period, they were not always deployed at the same locations (see the Methods). Hence, we could not examine long-term trends in throughfall and litterfall loadings as we did for wet loadings of THg in the open.

THg dry loadings were quite variable across the heterogeneous boreal mixed wood forested landscape at the ELA. Using the "direct" method of estimating the dry deposition (throughfall + litterfall loadings − open area loadings), we calculated that the annual dry deposition of THg was 20.2 ± 4.9, 11.2 ± 2.2, 8.9 ± 1.6, and 15.9 ± 3.4 μg m^{-2} under the old growth, jack pine, deciduous, and wetland forest canopies, respectively, 2.7 to 6.1 times higher than wet THg loadings in adjacent open areas (Figure 1). As expected, the total THg dry deposition was highest under the old growth canopy, where LAI was also the highest (2.24 ± 1.54) relative to the other canopy types, where LAIs ranged only between 1.21 ± 0.98 and 1.41 ± 0.76.[17] Our measured annual dry deposition loadings of THg to the remote ELA landscape were similar to those comparably quantified in other North American forested locations (13−34 μg m^{-2}) but generally lower than those comparably quantified in European and Scandinavian forested sites (19−48 μg m^{-2}), whereas dry/wet loading ratios at the ELA were within the range of those measured at those other sites (1.5−10.4) (e.g., table 3 in ref 14).

The majority of Hg in forest canopies is thought to originate from the foliar uptake of GEM through stomata (although see further discussion below) as well as some direct dry deposition of GOM and PBM to foliar surfaces.[7,8,24] Although a portion of this Hg is subsequently deposited to the forest floor via litterfall and washoff in throughfall, another portion may be re-emitted to the atmosphere as GEM following Hg(II) photoreduction on foliar surfaces.[25] For example, Graydon et al.[17] used a combined Geographical Information System and mass-balance-based approach to quantify the fate of experimentally applied upland (^{200}Hg) and wetland (^{198}Hg) spike to forest canopies within the METAALICUS catchment (2001−2006). The largest flux of Hg from the canopy over a 1 year postapplication period was from photoreduction and GEM emission to the atmosphere (upland: 45%; wetland: 71%). As such, the photoreduction and the emission to the atmosphere may prevent a portion of the Hg initially deposited to forest canopies from ever reaching the forest floor. Furthermore, whereas deciduous tree foliage senesces annually, in their northernmost ranges, coniferous trees such as *P. banksiana*, *Picea* sp., and *Abies* sp. can retain their foliage for up to 5.5, 15, and 9 years, respectively.[26] As such, annual Hg loadings in litterfall under coniferous tree canopies integrate multiple years of Hg loadings to the canopy itself.

Atmospheric Concentrations of GEM, GOM, and PBM. *GEM.* During the 2005−2013 sampling period, average 3 h GEM concentrations ranged between 0.40 and 8.24 ng m^{-3} (Figure 2), within the range of mean GEM concentrations measured at numerous locations around the globe (e.g., 0.86 to 2.93 ng m^{-3} in ref 27). The mean annual GEM concentrations (±S.E.) were the highest during our first full year of measurements in 2006 (1.62 ± 0.003 ng m^{-3}), decreased to a low in 2009 (1.21 ± 0.002 ng m^{-3}), and then began rising again until our final full year of measurements in 2012 (1.38 ± 0.002 ng m^{-3}) (Figure 3). Using all data from 2005 to 2013, there was an overall decline in GEM concentrations of 2.2 ± 0.06% yr^{-1}, consistent with declines observed at numerous other global sites.[28] However, the increase in mean annual GEM concentrations at the ELA between 2010 and 2012 suggests that there was an emerging and new source of GEM to the region. Although GEM emissions in North America declined between 2000 and 2010 (e.g., ref 29), total global GEM emissions began increasing again in 2010, driven primarily by increasing Hg emissions in East and South Asia and Africa that more than offset emission reductions in North America.[30] With a mean atmospheric residence time of 6 to 24 months,[31] GEM emitted to the atmosphere appeared to be well enough mixed that we were able to detect the increase even at our remote site in central Canada.

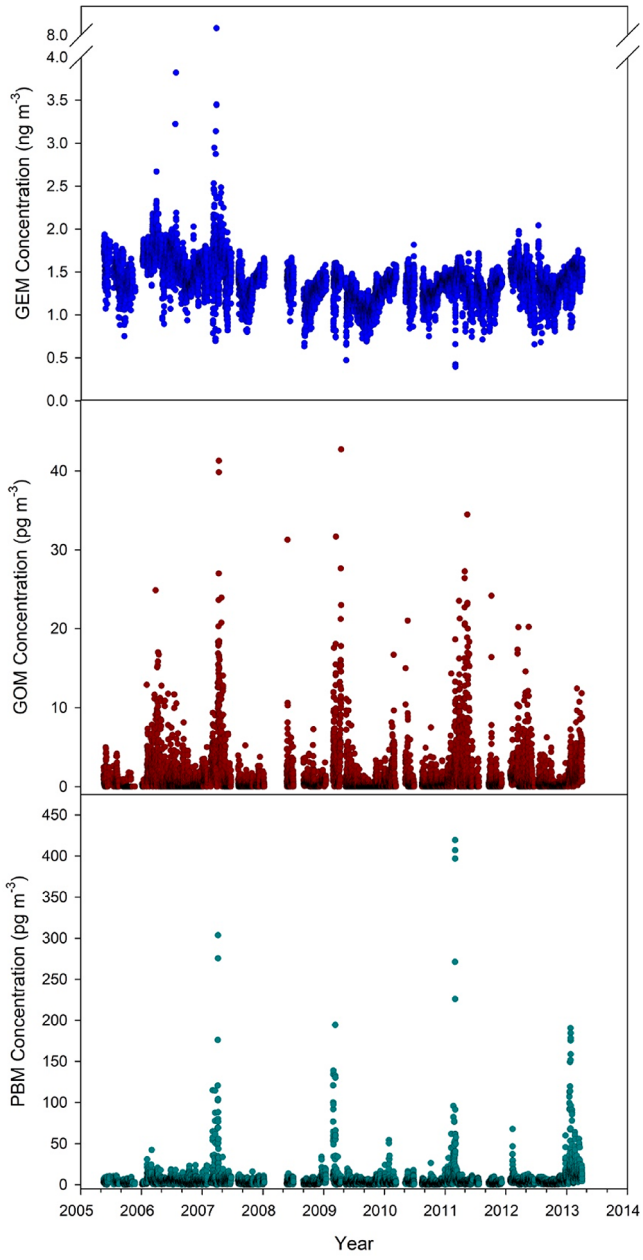

Figure 2. Atmospheric concentrations of gaseous elemental Hg (GEM), gaseous oxidized Hg (GOM), and particulate bound Hg (PBM) (3 h means) measured at the Experimental Lakes Area meteorological site (2005−2013).

There were also very pronounced seasonal patterns in atmospheric concentrations of GEM (Figures 4 and 5 and

DOI: 10.1021/acs.est.9b01338
Environ. Sci. Technol. 2019, 53, 8017−8026

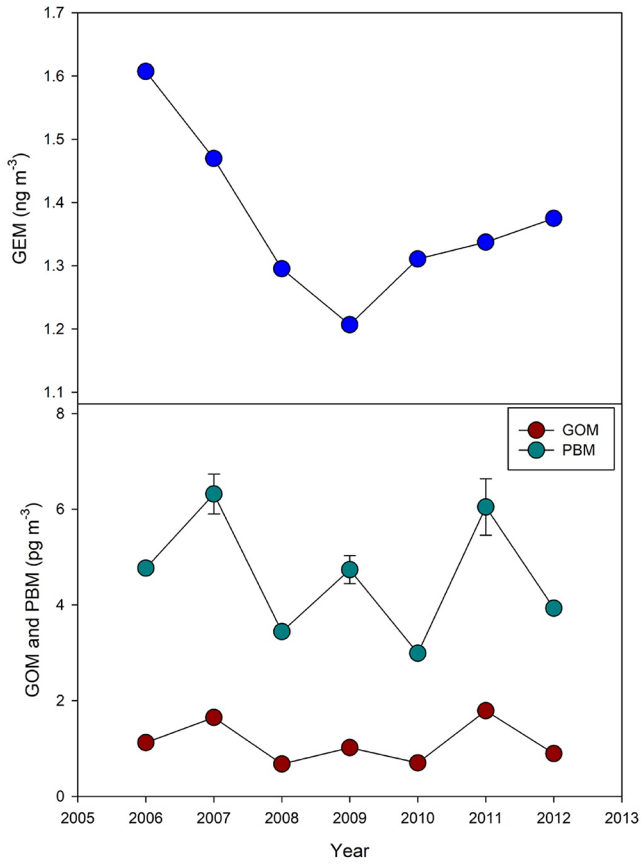

Figure 3. Mean (±S.E., when large enough to be visible) annual atmospheric concentrations of gaseous elemental Hg (GEM), gaseous oxidized Hg (GOM), and particulate bound Hg (PBM) measured at the Experimental Lakes Area meteorological site (full years 2006–2012).

Figure S4), where at the ELA, seasons were defined as winter (November 1 to April 30; daily freezing temperatures with snow on the ground and lakes with ice cover); spring (May 1–31; lakes becoming ice-free and deciduous canopy green-up); summer (June 1–September 30; plant growth and lake open water season); and fall (October 1–31; annual plant senescence and prior to lake freeze-up and snow accumulation). Mean GEM concentrations (±S.E.) were highest in the winter (1.47 ± 0.002 ng m^{-3}) and spring (1.44 ± 0.004 ng m^{-3}), lower in the summer (1.34 ± 0.002 ng m^{-3}), and lowest in the fall (1.24 ± 0.002 ng m^{-3}). Mean monthly GEM concentrations peaked in March (1.57 ± 0.007 ng m^{-3}) and were lowest in September (1.22 ± 0.003 ng m^{-3}). This general seasonal pattern in GEM concentrations was also seen at numerous other monitoring locations in Canada.[32]

There was no overall relationship between wind direction (weighted by wind speed) at the time of sampling and high concentrations of GEM (Figure S5). This finding suggests that the relatively remote ELA site is not immediately impacted by single-point sources of Hg emissions. Using principal component analyses (PCAs; run using the package *vegan*[33] in R[34]) that integrated mean daily GEM (and GOM and PBM) concentrations with mean daily concentrations of other atmospheric gaseous and particulate species quantified at the ELA meteorological site by the Air Quality Research Division of ECCC (Combined Atmospheric Gases and Particles data set;[35] also see ref 36) (Figure S6), we found that between 2005 and 2012, atmospheric concentrations of GEM varied in concert with atmospheric concentrations of gaseous HNO_3 and particulate-bound SO_4^{2-} and NH_4^+ (Figure 5). These relationships suggest that there were likely anthropogenic sources of GEM from the burning of fossil fuels for power production or transportation, especially during the colder months of the year, that made their way to the ELA. GEM

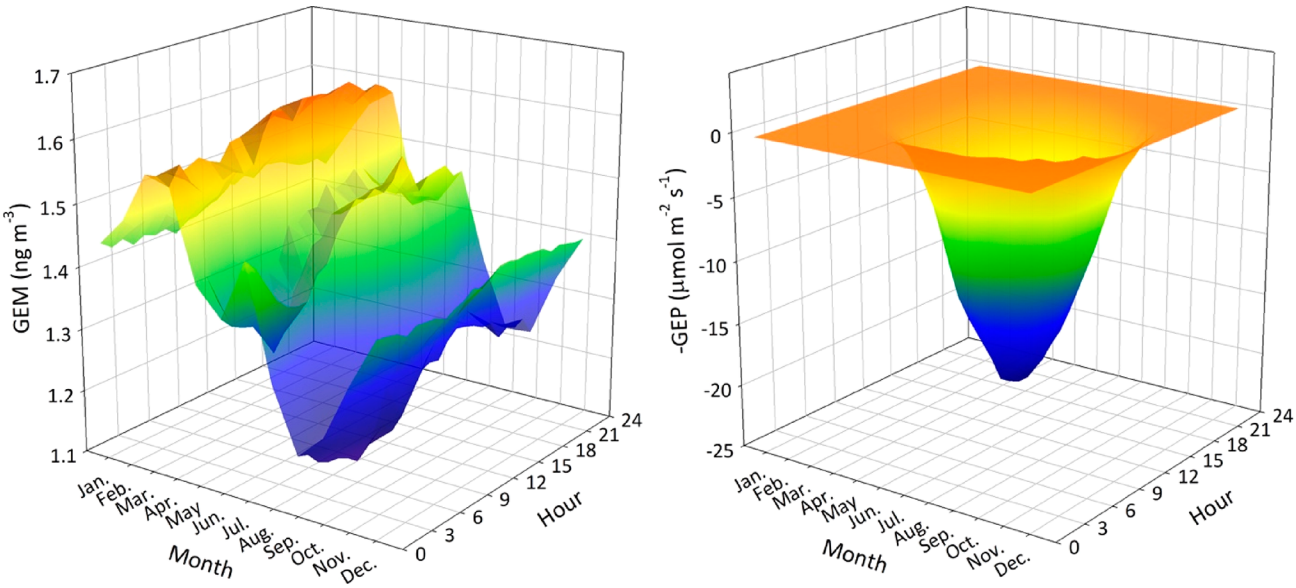

Figure 4. Three-dimensional plot of average hourly gaseous elemental Hg (GEM) concentrations averaged for each month of the year at the Experimental Lakes Area (ELA) meteorological site (2005–2013) (left) and average hourly gross ecosystem productivity (GEP) averaged for each month of the year at a similar mixedwood boreal forest near Timmins, Ontario (AmeriFlux Site Ca-Gro) (2006–2012) (right). GEP is plotted on a negative scale for better visual interpretation with the GEM plot. Color gradations represent gradations in GEM concentrations and rates of GEP. See Figure 5 and Figure S4 for the 2D versions of the GEM plot. Also see Figure S7 for 2D plots of GEM versus GEP, ecosystem respiration, and net ecosystem productivity (the net balance between GEP and ER).

DOI: 10.1021/acs.est.9b01338
Environ. Sci. Technol. 2019, 53, 8017–8026

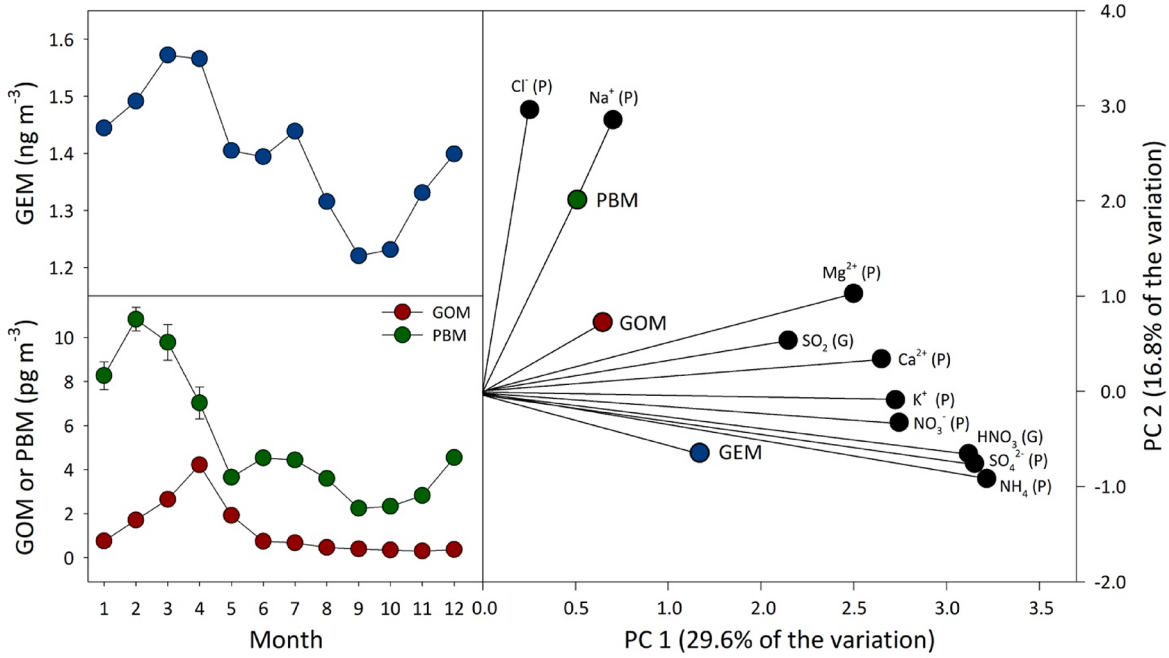

Figure 5. Left graphs: Mean (±S.E., when large enough to be visible) monthly atmospheric concentrations of gaseous elemental Hg (GEM), gaseous oxidized Hg (GOM), and particulate bound Hg (PBM) measured at the Experimental Lakes Area meteorological site (2005−2013). Right graph: Results from a principal component analyses of daily concentrations of GEM, GOM, PBM, a variety of particulate-bound (P) cation and anions, and gaseous (G) SO_2 and HNO_3.

concentrations then declined throughout the summer and fall. Together, PC1 and PC2 accounted for 46.4% of the variation.

Jiskra et al.[37] recently documented that at inland sites in the northern hemisphere, GEM concentrations generally covaried with atmospheric concentrations of CO_2, with concentration minimums of both GEM and CO_2 occurring during the summer when GEP and CO_2 assimilation by photosynthesizing vegetation was greatest. Hence, it was proposed that terrestrial vegetation acts as a GEM pump, whereby photosynthesis controls seasonal variations in global atmospheric GEM concentrations through stomatal uptake.[37] Although this relationship may generally hold true for the Northern Hemisphere as a whole, at the ELA meteorological station, surrounded by expansive regions of boreal mixedwood forests, it did not (Figure 4 and Figure S7). Diel and annual patterns in GEP, a better proxy for stomatal conductance than CO_2 concentrations alone, were estimated between 2006 and 2012 from long-term eddy covariance flux measurements at the AmeriFlux Groundhog River research site near Timmins, Ontario (48°13.01′ N; 82°9.2′ W).[38] This nearest AmeriFlux site to the ELA was situated in a similar boreal mixedwood forest approximately 1° S and 11° E of the ELA (Figure S1). For this site, hourly measurements of net ecosystem exchange of CO_2 were partitioned into GEP and ecosystem respiration (ER) using air temperature and shortwave radiation response curves following methods described by Humphreys et al. (2014).[39] Average hourly and monthly patterns of GEP were exactly as expected (minimums at night and during winter, maximums at midday and during summer) but did not overall match our average hourly and monthly patterns of GEM concentrations (Figure 4). In fact, during the growing seasons in the spring and summer, there was a positive relationship between the GEM concentrations measured at the ELA and the rates of GEP, ER, and net ecosystem productivity (NEP; the net balance between GEP and ER) estimated from the nearest AmeriFlux site (Figure S7), counterintuitive to expectations if vegetation had assimilated GEM during stomatal conductance. These results suggest that GEP and ER, or drivers of GEP and ER (such as solar radiation and temperature), enhance GEM emission from forested landscapes.

Overall, at our site, GEM concentrations were highest with little daily variation in the winter and lower and more dynamic in the summer. However, concentrations of GEM continued to decline into the autumn. During all seasons, average hourly GEM concentrations were lowest from 4:00 to 8:00 and highest between 14:00 and 18:00 (Figure 4 and Figure S4). Diel patterns in GEM concentrations were most pronounced in the summer, followed by the spring and fall, and muted during the winter. As such, diel patterns in concentrations of GEM at our site were likely consistent with a combination of: (1) the nighttime deposition of GEM from the shallow nocturnal boundary layer, followed by mixing with more GEM-rich air aloft when the nocturnal inversion broke down; (2) the daytime surface emission of GEM following photolytic or temperature-driven processes on foliage surfaces, soils, or snow; and (3) the bidirectional exchange of GEM through leaf stomata.[16] These factors help to explain a general pattern of weak GEM deposition during the night, higher deposition in early mornings, net daytime GEM emissions, followed by deposition again in the evening. Cold temperatures, dormant vegetation, and slowed microbial activity likely muted the magnitude of diel variation in GEM concentrations during winter.[16]

GOM and PBM. Concentrations of GOM and PBM were almost three orders of magnitude lower than GEM concentrations, ranging from below detection concentrations for both species to 42.7 and 419 pg m^{-3}, respectively, during our 2005−2013 measurement period (Figure 2). Mean annual GOM concentrations were quite low, ranging between 0.68 ±

DOI: 10.1021/acs.est.9b01338
Environ. Sci. Technol. 2019, 53, 8017−8026

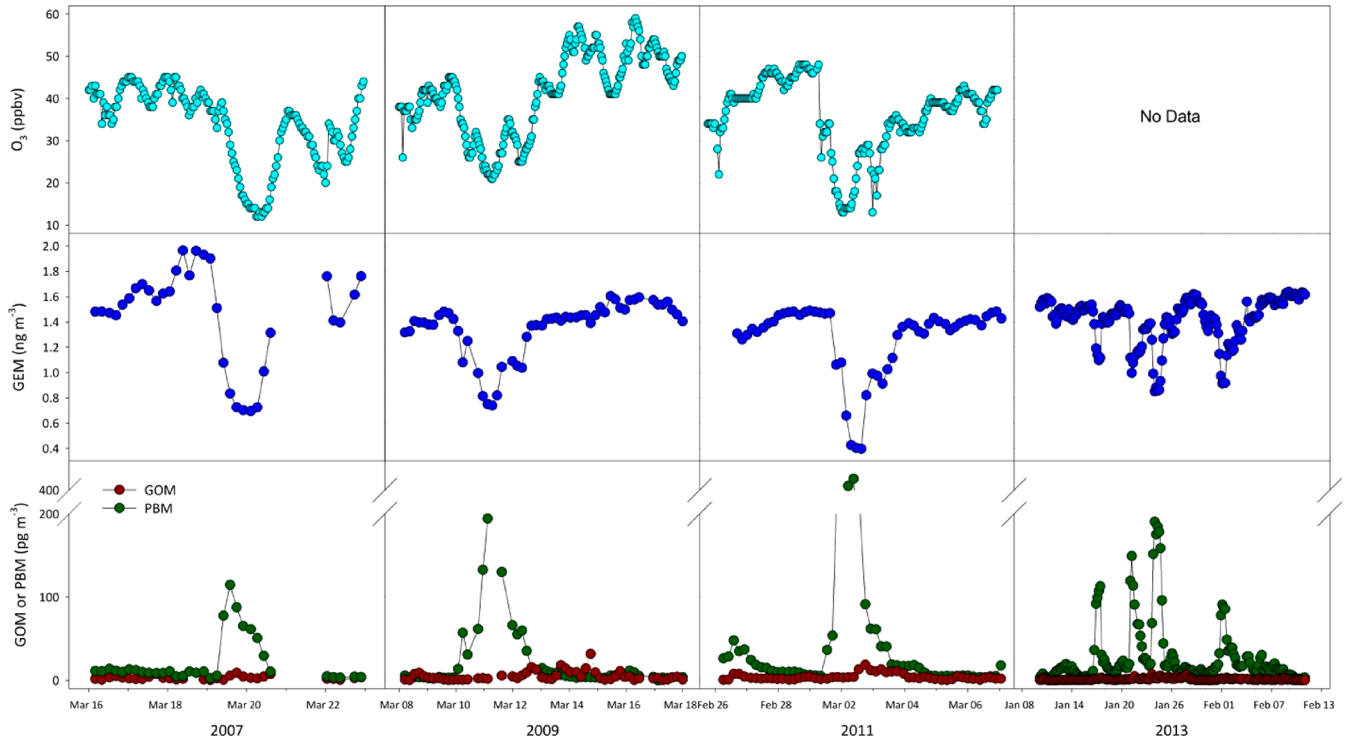

Figure 6. Atmospheric concentrations of ozone (O_3), gaseous elemental Hg (GEM), gaseous oxidized Hg (GOM), and particulate bound Hg (PBM) measured at the Experimental Lakes Area meteorological site during four periods in 2007, 2009, 2011, and 2013 when concentrations of GEM were observed to be rapidly and uncharacteristically depleted. Also, see Figure S11 for air mass back trajectories during these periods.

0.05 pg m^{-3} (2008) and 1.79 ± 0.09 pg m^{-3} (2011) (Figure 3). Mean annual PBM concentrations were slightly higher but ranged only between 2.99 ± 0.10 pg m^{-3} (2010) and 6.32 ± 0.42 pg m^{-3} (2007) (Figure 3). Unlike for concentrations of GEM, there were no observable patterns of change in mean annual PBM or GOM concentrations over the years we sampled (Figure 3). There were also no overall relationships between wind direction (weighted by wind speed) at the time of sampling and high concentrations of GOM and PBM (Figure S5). However, there were pronounced seasonal patterns in PBM and GOM concentrations (Figure 5). Mean PBM concentrations were the highest in the winter (8.40 ± 0.32 pg m^{-3}) and then declined through the spring (5.13 ± 0.33 pg m^{-3}), summer (4.18 ± 0.05 pg m^{-3}), and fall (2.46 ± 0.04 pg m^{-3}). Mean GOM concentrations were the highest in spring (2.92 ± 0.12 pg m^{-3}), followed by winter (1.41 ± 0.04 pg m^{-3}), summer (0.63 ± 0.02 pg m^{-3}), and fall (0.34 ± 0.01 pg m^{-3}). PBM concentrations peaked in February (10.8 ± 0.54 pg m^{-3}), whereas GOM concentrations peaked in April (4.22 ± 0.21 pg m^{-3}).

This seasonal offset in which PBM concentrations peak prior to GOM has been found elsewhere, for example, in both coastal high (Alert, Nunavut)[40] and low (Churchill, Manitoba)[41] Arctic regions in Canada. Previous field and modeling studies have suggested that factors such as relative humidity (RH), air temperature, wind speed, air mass origin, and aerosol particle loadings may impact the partitioning of Hg species.[22,42−46] For example, in Alert, high PBM concentrations occurred in the spring, when high particle concentrations were present from Arctic haze and sea salt aerosols.[40] Furthermore, prior to the transition from a higher ratio of PBM to a higher ratio of GOM, the median air temperature and RH were −24.8 °C and 74%, whereas after the transition, the median air temperature and RH were −5.8 °C and 85%.[40] At the ELA, however, the mean monthly PBM fraction was significantly and positively correlated with the mean monthly RH, with no relationship to temperature (Figures S8 and S9), which is not surprising at our inland site distant from marine aerosol influences. Instead, we found, using the above-described PCA, that mean daily atmospheric concentrations of PBM covaried with mean daily concentrations of particulate Cl^- and Na^+ (Figure 5). Mean monthly concentrations of Cl^- and Na^+ began to rise in November, peaked in December and January, and returned to background by April (Figure S6), likely reflecting the patterns in winter road salt use[47] and its atmospheric dispersion postapplication,[48] even though the two nearest roadways (Highway 17 (the Trans-Canada Highway) and Highway 71) were ∼25 km north and west of the ELA meteorological site. Whether PBM was a component of road salt/sand applied to the highways or produced from the oxidation of GEM via heterogeneous reactions with chlorine atoms should be the subject of future research. Mean daily atmospheric concentrations of GOM, on the contrary, covaried with mean daily concentrations of particulate Mg^{2+} and Ca^{2+} and gaseous SO_2 (Figure 5), suggesting both mineral-related sources of GOM dispersed by aeolian processes and anthropogenic-related sources of GOM from the combustion of fossil fuels.

Forest Fires. Distant and nearby forest fires occasionally resulted in smoke-filled air masses being delivered to the ELA. Although smoky days at the ELA were not specifically recorded during our measurement period, we were able to examine the impact of forest fires on atmospheric concentrations of GEM, GOM, and PBM during one occasion when a large forest fire ignited within 10 km of the ELA meteorological station on June 20, 2006. For 11 days prior to that forest fire, mean

DOI: 10.1021/acs.est.9b01338
Environ. Sci. Technol. 2019, 53, 8017−8026

concentrations of GEM, GOM, and PBM were 1.69 ± 0.14 ng m^{-3}, 1.28 ± 2.09 pg m^{-3}, and 4.23 ± 2.16 pg m^{-3}, respectively (Figure S10). For the 11 days following the start of the fire, during which there was heavy smoke in the air, GEM and PBM concentrations increased, and became more variable, to 1.77 ± 0.36 ng m^{-3} and 6.28 ± 2.75 pg m^{-3}, likely due to the pyroreduction of Hg in vegetation to GEM and the release of incompletely burned organic particulate matter during the fire.[49] Concentrations of GOM decreased, though, to 1.07 ± 1.60 pg m^{-3}, likely because a portion of the GOM was scavenged by the particulate matter in smoke (Figure S10). However, only the changes in PBM concentrations were significantly different (Type III ANOVA; $F = 11.9$, $p < 0.001$).

Depleted Atmospheric Concentrations of GEM and Ozone (O_3) at the ELA. We observed rapid and uncharacteristic depletions of atmospheric concentrations of GEM, with a corresponding rise in concentrations of PBM, but not GOM, on four occasions during our measurement period, all of which appeared during the colder months of January through March (Figure 6). On three of those occasions, when data were available, we also observed a corresponding rapid depletion in atmospheric concentrations of O_3 (Figure 6). In polar regions following polar sunrise in the spring, heterogeneous cold reactions that oxidize GEM to GOM and Hg(II) bound to particles (i.e., PBM) are driven by marine halogens such as bromine, which also catalytically destroy tropospheric O_3.[50] These atmospheric Hg depletion events (AMDEs) typically do not occur as far inland and south as the ELA, even though Thornton et al.[51] observed the chlorine atom precursor nitryl chloride at a midcontinental site 1400 km from the nearest coastline, suggesting that a significant fraction of tropospheric chlorine atoms may arise directly from anthropogenic pollutants. Hence, we calculated back trajectories using HYSPLIT[52] to determine from where air masses originated during the occasions we observed depleted atmospheric concentrations of O_3 and GEM, with a corresponding rise in concentrations of PBM, at the ELA. In all cases, air masses originated from either Hudson Bay[41] or the Beaufort Sea (e.g., Barrow, Alaska[50,53]), where AMDEs are known to occur (Figure S11). As such, we believe that air masses already depleted in O_3 and GEM, but enriched in PBM, were transported to the ELA during the four occasions, rather than AMDEs actually occurring at the ELA. As described above, the offset in which PBM concentrations peak prior to GOM concentrations during the Arctic AMDE period corresponds well with the timing in which we observed corresponding elevated concentrations of PBM, but not GOM, at the ELA (late January to March).

Modeled Dry Deposition. Modeled V_d values for GEM ranged between 0.01 cm s^{-1} in the winter and 0.07 cm s^{-1} during the summer. Modeled V_d values for combined GOM and PBM ranged between near 0 cm s^{-1} in the winter and 4.5 cm s^{-1} during the summer.[20] Because GEM concentrations were on average three orders of magnitude higher than GOM concentrations, modeled dry loadings of GEM (<0.01 to ∼2.5 ng m^2 h^{-1}) were almost double those of modeled dry loadings of GOM (0.0 to ∼1 ng m^2 h^{-1}), with seasonal deposition patterns more reflecting seasonal patterns in dry deposition velocities than seasonal patterns in GEM and GOM concentrations. Modeled dry loadings of PBM were fairly insignificant at <0.05 ng m^2 h^{-1}.

The range of empirically calculated annual dry THg loadings at the ELA (14.7 to 16.4 μg m^{-2}) was consistent with annual dry THg loadings of 9 to 20 μg m^{-2} actually measured under forest canopies using the direct method of subtracting wet THg loadings in the open from THg loadings in throughfall plus litterfall (Figure 1). Because of the forest-type inputs used in the model, modeled dry THg loadings were, as expected, more consistent with measured dry deposition in the old growth and wetland forests than under the fire-regenerating jack pine or deciduous forests (Figure 1).

We compared the empirically estimated dry deposition fluxes to results from the nested GEOS-Chem simulation over the ELA (Figure S12).[21] In the GEOS-Chem simulation, on the basis of the standard resistance in the series model, THg dry deposition loadings were 4.5 to 5.0 times higher than measured THg wet deposition loadings in the open at the ELA (3.3 ± 1.6 μg m^{-2}). These results are similar to the 2.7 to 6.1 times higher THg dry deposition actually measured under the various boreal mixedwood canopies at the ELA, suggesting that existing dry deposition schemes in the model reasonably capture the uptake of GEM in terrestrial ecosystems.

Moving Forward. Using our long-term data sets, we showed that dry THg loadings under forest canopies in throughfall and litterfall are 2.7 to 6.1 times greater than wet THg loadings in the open. Because the majority of the dry THg load is from GEM deposition, as our long-term measurement record and modeling both show, measured regional atmospheric GEM concentrations could be used to accurately estimate dry THg loading rates to regional watersheds. The North American National Atmospheric Deposition Program Atmospheric Mercury Network (NADP AMNet) has explored using Zhang et al's.[20,21] methodology (measured Tekran concentrations and modeled V_d values) to estimate dry Hg deposition to North America watersheds.[54] Our study gives confidence for this technique. However, future modeling approaches will benefit from refining resistances in dry deposition schemes to reflect Hg specific values and calculate fluxes of different atmospheric Hg species through separate deposition pathways to foliage interiors and surfaces. Although detailed measurements, such as those made here, provide invaluable information on certain drivers of Hg dry loadings to watersheds and hourly and seasonal variations in atmospheric concentrations of GEM, GOM, and PBM, much more research is required to fully understand how, for example, the rates of GEP and ER affect regional atmospheric concentrations of Hg and Hg dry loading rates. It is essential that this is done across a wide range of watershed and vegetation types in conjunction with actual Hg dry loading measurements that can be used for model evaluation.

■ ASSOCIATED CONTENT

Supporting Information

The Supporting Information is available free of charge on the ACS Publications website at DOI: 10.1021/acs.est.9b01338.

Extended methods sections, 12 additional figures supporting the main text, and references (PDF)

■ AUTHOR INFORMATION

Corresponding Author

*Phone: 780-492-9386; e-mail: vince.stlouis@ualberta.ca.

ORCID

Vincent L. St. Louis: 0000-0001-5405-1522

Helen M. Amos: 0000-0002-0297-6643

Elsie M. Sunderland: 0000-0003-0386-9548

DOI: 10.1021/acs.est.9b01338
Environ. Sci. Technol. 2019, 53, 8017−8026

Kyra A. St. Pierre: 0000-0003-0981-920X

Notes

The authors declare no competing financial interest.

■ ACKNOWLEDGMENTS

Dry deposition coding was provided by Leiming Zhang, Paige Wright, and Zhiyong Wu. We thank summer students Shawn Harriman, Jasmin Finch, Joanna Januszkiewicz, Eric Ong, Sarah Downey, and Linnea Mowat. We also greatly appreciate field and laboratory help from Justin Shead, Brian Dimock, Sara Berkel, Z McLatcher, Po Yee Chan, April Zembal, and Caroline Lee. On-site checks and maintenance of the Tekran instrumentation was provided by Justin Shead, Alexis Burt, Kim Palmquist, Lynn Dupuis, and Gerald Fitzgerald. We thank Amanda Cole, Rosa Wu, and James Kuchta from Environment and Climate Change Canada (ECCC) for providing the CAPMoN combined atmospheric gases and particles datasets. We acknowledge Harry McCaughey and the principal funders of the Groundhog River Flux Station (CA-Gro) for the provision of CO_2 flux data plus ancillary meteorological and ecological data from this mixedwood boreal site, retrieved in January 2019 from the Ameriflux database. Studio X Design, Inc. (Edmonton, Alberta) created Figure [1]. This project received real or in-kind funding from the Natural Sciences and Engineering Research Council of Canada (NSERC), Manitoba Hydro, Collaborative Mercury Research Network (COMERN), ECCC, Canadian Circumpolar Institute, Electric Power Research Institute (EPRI), and the Department of Fisheries and Oceans Canada.

■ REFERENCES

(1) Obrist, D.; Kirk, J. L.; Zhang, L.; Sunderland, E. M.; Jiskra, M.; Selin, N. E. A review of global environmental mercury processes in response to human and natural perturbations: Changes of emissions, climate, and land use. *Ambio* **2018**, *47* (2), 116−140.

(2) Kessler, R. The Minamata Convention on Mercury: a first step toward protecting future generations. *Environ. Health Persp.* **2013**, *121* (11), A304−A309.

(3) Harris, R. C.; Rudd, J. W. M.; Amyot, M.; Babiarz, C. L.; Beaty, K. G.; Blanchfield, P. J.; Bodaly, R. A.; Branfireun, B. A.; Gilmour, C. C.; Graydon, J. A.; Heyes, A.; Hintelmann, H.; Hurley, J. P.; Kelly, C. A.; Krabbenhoft, D. P.; Lindberg, S. E.; Mason, R. P.; Paterson, M. J.; Podemski, C. L.; Robinson, A.; Sandilands, K. A.; Southworth, G. R.; St. Louis, V. L.; Tate, M. T. Whole-ecosystem study shows rapid fish-mercury response to changes in mercury deposition. *Proc. Natl. Acad. Sci. U. S. A.* **2007**, *104* (42), 16586.

(4) Knightes, C. D.; Sunderland, E. M.; Barber, M. C.; Johnston, J. M.; Ambrose, R. B., Jr. Application of ecosystem-scale fate and bioaccumulation models to predict fish mercury response times to changes in atmospheric deposition. *Environ. Toxicol. Chem.* **2009**, *28* (4), 881−893.

(5) Rudd, J. W. M.; Bodaly, R. A.; Fisher, N. S.; Kelly, C. A.; Kopec, D.; Whipple, C. Fifty years after its discharge, methylation of legacy mercury trapped in the Penobscot Estuary sustains high mercury in biota. *Sci. Total Environ.* **2018**, *642*, 1340−1352.

(6) Graydon, J. A.; St. Louis, V. L.; Hintelmann, H.; Lindberg, S. E.; Sandilands, K. A.; Rudd, J. W. M.; Kelly, C. A.; Tate, M. T.; Krabbenhoft, D. P.; Lehnherr, I. Investigation of Uptake and Retention of Atmospheric Hg(II) by Boreal Forest Plants Using Stable Hg Isotopes. *Environ. Sci. Technol.* **2009**, *43* (13), 4960−4966.

(7) Enrico, M.; Roux, G. L.; Marusczak, N.; Heimbürger, L.-E.; Claustres, A.; Fu, X.; Sun, R.; Sonke, J. E. Atmospheric Mercury Transfer to Peat Bogs Dominated by Gaseous Elemental Mercury Dry Deposition. *Environ. Sci. Technol.* **2016**, *50* (5), 2405−2412.

(8) Demers, J. D.; Blum, J. D.; Zak, D. R. Mercury isotopes in a forested ecosystem: Implications for air-surface exchange dynamics and the global mercury cycle. *Global Biogeochem. Cycles* **2013**, *27* (1), 222−238.

(9) Obrist, D.; Agnan, Y.; Jiskra, M.; Olson, C. L.; Colegrove, D. P.; Hueber, J.; Moore, C. W.; Sonke, J. E.; Helmig, D. Tundra uptake of atmospheric elemental mercury drives Arctic mercury pollution. *Nature* **2017**, *547*, 201−204.

(10) Enrico, M.; Le Roux, G.; Heimbürger, L.-E.; Van Beek, P.; Souhaut, M.; Chmeleff, J.; Sonke, J. E. Holocene Atmospheric Mercury Levels Reconstructed from Peat Bog Mercury Stable Isotopes. *Environ. Sci. Technol.* **2017**, *51* (11), 5899−5906.

(11) Grigal, D. F.; Kolka, R. K.; Fleck, J. A.; Nater, E. A. Mercury budget of an upland-peatland watershed. *Biogeochemistry* **2000**, *50* (1), 95−109.

(12) St. Louis, V. L.; Rudd, J. W. M.; Kelly, C. A.; Hall, B. D.; Rolfhus, K. R.; Scott, K. J.; Lindberg, S. E.; Dong, W. Importance of the Forest Canopy to Fluxes of Methyl Mercury and Total Mercury to Boreal Ecosystems. *Environ. Sci. Technol.* **2001**, *35* (15), 3089−3098.

(13) Demers, J. D.; Driscoll, C. T.; Fahey, T. J.; Yavitt, J. B. Mercury Cycling in Litter and Soil in Different Forest Types in the Adirondack Region, New York, USA. *Ecol. Appl.* **2007**, *17* (5), 1341−1351.

(14) Graydon, J. A.; St. Louis, V. L.; Hintelmann, H.; Lindberg, S. E.; Sandilands, K. A.; Rudd, J. W. M.; Kelly, C. A.; Hall, B. D.; Mowat, L. D. Long-Term Wet and Dry Deposition of Total and Methyl Mercury in the Remote Boreal Ecoregion of Canada. *Environ. Sci. Technol.* **2008**, *42* (22), 8345−8351.

(15) Wesely, M. L. Parameterization of surface resistances to gaseous dry deposition in regional-scale numerical models. *Atmos. Environ. (1967-1989)* **1989**, *23* (6), 1293−1304.

(16) Zhang, L.; Wright, L. P.; Blanchard, P. A review of current knowledge concerning dry deposition of atmospheric mercury. *Atmos. Environ.* **2009**, *43* (37), 5853−5864.

(17) Graydon, J. A.; St. Louis, V. L.; Lindberg, S. E.; Sandilands, K. A.; Rudd, J. W. M.; Kelly, C. A.; Harris, R.; Tate, M. T.; Krabbenhoft, D. P.; Emmerton, C. A.; Asmath, H.; Richardson, M. The role of terrestrial vegetation in atmospheric Hg deposition: Pools and fluxes of spike and ambient Hg from the METAALICUS experiment. *Global Biogeochem. Cycles* **2012**, *26* (1), GB1022.

(18) Steffen, A.; Scherz, T.; Olson, M.; Gay, D. A.; Blanchard, P. A comparison of data quality control protocols for atmospheric mercury speciation measurements. *J. Environ. Monit.* **2012**, *14* (3), 752−765.

(19) Wright, L. P.; Zhang, L. An approach estimating bidirectional air-surface exchange for gaseous elemental mercury at AMNet sites. *J. Adv. Model. Earth Syst.* **2015**, *7* (1), 35−49.

(20) Zhang, L.; Brook, J. R.; Vet, R. A revised parameterization for gaseous dry deposition in air-quality models. *Atmos. Chem. Phys.* **2003**, *3* (6), 2067−2082.

(21) Zhang, L.; Blanchard, P.; Gay, D. A.; Prestbo, E. M.; Risch, M. R.; Johnson, D.; Narayan, J.; Zsolway, R.; Holsen, T. M.; Miller, E. K.; Castro, M. S.; Graydon, J. A.; Louis, V. L. S.; Dalziel, J. Estimation of speciated and total mercury dry deposition at monitoring locations in eastern and central North America. *Atmos. Chem. Phys.* **2012**, *12* (9), 4327−4340.

(22) Amos, H. M.; Jacob, D. J.; Holmes, C. D.; Fisher, J. A.; Wang, Q.; Yantosca, R. M.; Corbitt, E. S.; Galarneau, E.; Rutter, A. P.; Gustin, M. S.; Steffen, A.; Schauer, J. J.; Graydon, J. A.; Louis, V. L. S.; Talbot, R. W.; Edgerton, E. S.; Zhang, Y.; Sunderland, E. M. Gas-particle partitioning of atmospheric Hg(II) and its effect on global mercury deposition. *Atmos. Chem. Phys.* **2012**, *12* (1), 591−603.

(23) Risch, M. R.; Gay, D. A.; Fowler, K. K.; Keeler, G. J.; Backus, S. M.; Blanchard, P.; Barres, J. A.; Dvonch, J. T. Spatial patterns and temporal trends in mercury concentrations, precipitation depths, and mercury wet deposition in the North American Great Lakes region, 2002−2008. *Environ. Pollut.* **2012**, *161*, 261−271.

(24) Zheng, W.; Obrist, D.; Weis, D.; Bergquist, B. A. Mercury isotope compositions across North American forests. *Global Biogeochem. Cycles* **2016**, *30* (10), 1475−1492.

DOI: 10.1021/acs.est.9b01338
Environ. Sci. Technol. 2019, 53, 8017−8026

(25) Yuan, W.; Sommar, J.; Lin, C.-J.; Wang, X.; Li, K.; Liu, Y.; Zhang, H.; Lu, Z.; Wu, C.; Feng, X. Stable Isotope Evidence Shows Re-emission of Elemental Mercury Vapor Occurring after Reductive Loss from Foliage. *Environ. Sci. Technol.* **2019**, *53* (2), 651−660.
(26) Reich, P. B.; Rich, R. L.; Lu, X.; Wang, Y.-P.; Oleksyn, J. Biogeographic variation in evergreen conifer needle longevity and impacts on boreal forest carbon cycle projections. *Proc. Natl. Acad. Sci. U. S. A.* **2014**, *111* (38), 13703−13708.
(27) McLagan, D. S.; Mitchell, C. P. J.; Steffen, A.; Hung, H.; Shin, C.; Stupple, G. W.; Olson, M. L.; Luke, W. T.; Kelley, P.; Howard, D.; Edwards, G. C.; Nelson, P. F.; Xiao, H.; Sheu, G. R.; Dreyer, A.; Huang, H.; Abdul Hussain, B.; Lei, Y. D.; Tavshunsky, I.; Wania, F. Global evaluation and calibration of a passive air sampler for gaseous mercury. *Atmos. Chem. Phys.* **2018**, *18* (8), 5905−5919.
(28) Zhang, Y.; Jacob, D. J.; Horowitz, H. M.; Chen, L.; Amos, H. M.; Krabbenhoft, D. P.; Slemr, F.; St. Louis, V. L.; Sunderland, E. M. Observed decrease in atmospheric mercury explained by global decline in anthropogenic emissions. *Proc. Natl. Acad. Sci. U. S. A.* **2016**, *113* (3), 526−531.
(29) Weiss-Penzias, P. S.; Gay, D. A.; Brigham, M. E.; Parsons, M. T.; Gustin, M. S.; ter Schure, A. Trends in mercury wet deposition and mercury air concentrations across the U.S. and Canada. *Sci. Total Environ.* **2016**, *568*, 546−556.
(30) Streets, D. G.; Horowitz, H. M.; Lu, Z.; Levin, L.; Thackray, C. P.; Sunderland, E. M. Global and regional trends in mercury emissions and concentrations, 2010−2015. *Atmos. Environ.* **2019**, *201*, 417−427.
(31) Lindqvist, O.; Rodhe, H. Atmospheric mercury—a review. *Tellus B* **1985**, *37B* (3), 136−159.
(32) Cole, A. S.; Steffen, A.; Eckley, C. S.; Narayan, J.; Pilote, M.; Tordon, R.; Graydon, J. A.; St. Louis, V. L.; Xu, X.; Branfireun, B. A Survey of Mercury in Air and Precipitation across Canada: Patterns and Trends. *Atmosphere* **2014**, *5*, 635−668.
(33) Oksanen, J.; Blanchet, F. G.; Friendly, M.; Kindt, R.; Legendre, P.; McGlinn, D.; Minchin, P. R.; O'Hara, R. B.; Simpson, G. L.; Solymos, P.; Stevens, M. H. H.; Szoecs, E.; Wagner, H. *Package 'vegan'*, version 2.4-6, 2018.
(34) R Core Development Team. *R: A Language and Environment for Statistical Computing*; R Foundation for Statistical Computing: Vienna, Austria, 2016.
(35) Environment and Climate Change Canada. Monitoring of Combined Atmospheric Gases and Particles. 2018. http://donnees.ec.gc.ca/data/air/monitor/monitoring-of-combined-atmospheric-gases-and-particles/?lang=en (accessed January 30, 2019).
(36) Sirois, A.; Fricke, W. Regionally representative daily air concentrations of acid-related substances in Canada; 1983−1987. *Atmos. Environ., Part A* **1992**, *26* (4), 593−607.
(37) Jiskra, M.; Sonke, J. E.; Obrist, D.; Bieser, J.; Ebinghaus, R.; Myhre, C. L.; Pfaffhuber, K. A.; Wängberg, I.; Kyllönen, K.; Worthy, D.; Martin, L. G.; Labuschagne, C.; Mkololo, T.; Ramonet, M.; Magand, O.; Dommergue, A. A vegetation control on seasonal variations in global atmospheric mercury concentrations. *Nat. Geosci.* **2018**, *11* (4), 244−250.
(38) McCaughey, J. H.; Pejam, M. R.; Arain, M. A.; Cameron, D. A. Carbon dioxide and energy fluxes from a boreal mixedwood forest ecosystem in Ontario, Canada. *Agric. For. Meteorol.* **2006**, *140* (1), 79−96.
(39) Humphreys, E. R.; Charron, C.; Brown, M.; Jones, R. Two Bogs in the Canadian Hudson Bay Lowlands and a Temperate Bog Reveal Similar Annual Net Ecosystem Exchange of CO_2. *Arctic Antarctic Alpine Res.* **2014**, *46* (1), 103−113.
(40) Steffen, A.; Bottenheim, J.; Cole, A.; Ebinghaus, R.; Lawson, G.; Leaitch, W. R. Atmospheric mercury speciation and mercury in snow over time at Alert, Canada. *Atmos. Chem. Phys.* **2014**, *14* (5), 2219−2231.
(41) Kirk, J. L.; St. Louis, V. L. S.; Sharp, M. J. Rapid reduction and reemission of mercury deposited into snowpacks during atmospheric mercury depletion events at Churchill, Manitoba, Canada. *Environ. Sci. Technol.* **2006**, *40* (24), 7590−7596.
(42) Cobbett, F. D.; Steffen, A.; Lawson, G.; Van Heyst, B. J. GEM fluxes and atmospheric mercury concentrations (GEM, RGM and Hgp) in the Canadian Arctic at Alert, Nunavut, Canada (February−June 2005). *Atmos. Environ.* **2007**, *41* (31), 6527−6543.
(43) Steffen, A.; Douglas, T.; Amyot, M.; Ariya, P.; Aspmo, K.; Berg, T.; Bottenheim, J.; Brooks, S.; Cobbett, F.; Dastoor, A.; Dommergue, A.; Ebinghaus, R.; Ferrari, C.; Gardfeldt, K.; Goodsite, M. E.; Lean, D.; Poulain, A. J.; Scherz, C.; Skov, H.; Sommar, J.; Temme, C. A synthesis of atmospheric mercury depletion event chemistry in the atmosphere and snow. *Atmos. Chem. Phys.* **2008**, *8* (6), 1445−1482.
(44) Steen, A. O.; Berg, T.; Dastoor, A. P.; Durnford, D. A.; Engelsen, O.; Hole, L. R.; Pfaffhuber, K. A. Natural and anthropogenic atmospheric mercury in the European Arctic: a fractionation study. *Atmos. Chem. Phys.* **2011**, *11* (13), 6273−6284.
(45) Rutter, A. P.; Schauer, J. J. The effect of temperature on the gas−particle partitioning of reactive mercury in atmospheric aerosols. *Atmos. Environ.* **2007**, *41* (38), 8647−8657.
(46) Rutter, A. P.; Schauer, J. J. The Impact of Aerosol Composition on the Particle to Gas Partitioning of Reactive Mercury. *Environ. Sci. Technol.* **2007**, *41* (11), 3934−3939.
(47) Ontario Ministry of Transport. How Ontario's Highways Are Cleared in Winter. http://www.mto.gov.on.ca/english/ontario-511/winter-highway-maintenance.shtml (accessed January 30, 2019).
(48) Lazarcik, J.; Dibb, J. E. Evidence of Road Salt in New Hampshire's Snowpack Hundreds of Meters from Roadways. *Geosciences* **2017**, *7* (3), 54.
(49) Friedli, H. R.; Radke, L. F.; Lu, J. Y.; Banic, C. M.; Leaitch, W. R.; MacPherson, J. I. Mercury emissions from burning of biomass from temperate North American forests: laboratory and airborne measurements. *Atmos. Environ.* **2003**, *37* (2), 253−267.
(50) Moore, C. W.; Obrist, D.; Steffen, A.; Staebler, R. M.; Douglas, T. A.; Richter, A.; Nghiem, S. V. Convective forcing of mercury and ozone in the Arctic boundary layer induced by leads in sea ice. *Nature* **2014**, *506*, 81.
(51) Thornton, J. A.; Kercher, J. P.; Riedel, T. P.; Wagner, N. L.; Cozic, J.; Holloway, J. S.; Dubé, W. P.; Wolfe, G. M.; Quinn, P. K.; Middlebrook, A. M.; Alexander, B.; Brown, S. S. A large atomic chlorine source inferred from mid-continental reactive nitrogen chemistry. *Nature* **2010**, *464*, 271−274.
(52) Stein, A. F.; Draxler, R. R.; Rolph, G. D.; Stunder, B. J. B.; Cohen, M. D.; Ngan, F. NOAA's HYSPLIT Atmospheric Transport and Dispersion Modeling System. *Bull. Am. Meteorol. Soc.* **2015**, *96* (12), 2059−2077.
(53) Steffen, A.; Bottenheim, J.; Cole, A.; Douglas, T. A.; Ebinghaus, R.; Friess, U.; Netcheva, S.; Nghiem, S.; Sihler, H.; Staebler, R. Atmospheric mercury over sea ice during the OASIS-2009 campaign. *Atmos. Chem. Phys.* **2013**, *13* (14), 7007−7021.
(54) TDEP Ad Hoc Committee. Status Update and Re-Proposal AMNet Mercury Dry Deposition, 2017. http://nadp.slh.wisc.edu/committees/minutes/spring2017/tdep/HgDryDep.pdf (accessed March 2, 2019).

DOI: 10.1021/acs.est.9b01338
Environ. Sci. Technol. 2019, 53, 8017−8026